PCCP

PAPER

Cite this: *Phys. Chem. Chem. Phys.*, 2016, **18**, 9412

Detection of trapped charges in the blend films of polystyrene/SFDBAO electrets by electrostatic and Kelvin probe force microscopy†

Jin Wang,‡[a] Xiao Wang,‡[a] Wen-Juan Xu,[a] Ling-Hai Xie,*[a] Yu-Yu Liu,[a] Ming-Dong Yi[a] and Wei Huang*[ab]

Received 14th January 2016,
Accepted 1st March 2016

DOI: 10.1039/c6cp00273k

www.rsc.org/pccp

The charge trapping properties of the blend of polystyrene (PS) and a sterically hindered organic semiconductor SFDBAO (spiro[fluorene-9,7-dibenzo[*c*,*h*]acridin-5-one]) are investigated by electrostatic and Kelvin probe force microscopy (EFM and KPFM). EFM signals of trapped charge spots injected with controllable tip biases, which are recorded with different dissipation times *t*, the percent of SFDBAO in blends, and the scanning tip bias, have been measured. By the quantitative analysis, the excellent trapped charge density of PS/SFDBAO blend films for the holes ($\sim\times10^{-5}$ C m^{-2}) is much higher than that of the SFDBAO film ($\sim\times10^{-6}$ C m^{-2}) and the PS film ($\sim\times10^{-7}$ C m^{-2}). However, the trapped charge density of electrons ($\sim\times10^{-7}$ C m^{-2}) has the same order magnitude for SFDBAO, PS and the blend films. The results indicate that the blend of PS and SFDBAO enhances the high-density storage and retention abilities of the holes to a larger extent, but the endurance improvement of the electrons is not that obvious. By the KPFM measurement, we further verify the different diffusion rates of the trapped holes and electrons in the PS/SFDBAO blend films, and discuss the possible physical mechanism. The qualitative and quantitative determination of charge trapping properties in this work can be very useful for the characterization of PS/SFDBAO based charge trapping memory devices.

1. Introduction

Organic semiconductor films play a prominent role in the development of memory devices featuring flexibility, low cost, high storage density, fast response speed and long service life. A charge trapping memory (CTM) device based on organic semiconductor films has been regarded as a promising kind of non-volatile memory device.[1–3] The charge trapping process in organic semiconductor films strongly affects the device performance, such as the programme/erase speed, retention and threshold voltages.[4–6] Thus, searching for excellent charge trapping materials and investigating their electrical properties are essential ways to improve organic electronic devices. For example, researchers have constructed novel organic semiconductors to help improve the device performance.[7,8] Some reports have revealed the electrical properties of organic materials by techniques such as conductive atomic force microscopy (CAFM), scanning tunneling microscopy (STM), EFM and KPFM.[9–11] Among them, EFM and KPFM have been successfully used to visualize the spatial information of the trapped charge distribution and to offer high sensitivity not only for organic materials,[2,12–14] but also for inorganic materials.[15–18]

Recently, sterically hindered organic semiconductor molecule materials have shown great application potential in charge trapping memory.[7,19] Some research groups have reported that the steric hindrance may generate more charge trapping sites to improve the memory performances.[20,21] However, there is an incomplete understanding of the charge trapping properties of these organic semiconductor materials. In another study, we have researched the charge trapping properties of the sterically hindered organic semiconductor DSFXPY (1,6-di(spiro[fluorene-9,90-xanthene]-2-yl)pyrene) films by the EFM measurement.[22] We found that the charges can be easily injected into the DSFXPY film with a low voltage. However, the lateral spreading of trapped charges exhibited in previous work[2,12,15,23,24] was not observed in the DSFXPY film, revealing its promising localized

[a] *Key Laboratory for Organic Electronics and Information Displays & Institute of Advanced Materials (IAM), Jiangsu National Synergetic Innovation Center for Advanced Materials (SICAM), Nanjing University of Posts & Telecommunications, 9 Wenyuan Road, Nanjing 210023, China. E-mail: iamlhxie@njupt.edu.cn*

[b] *Key Laboratory of Flexible Electronics (KLOFE) & Institute of Advanced Materials (IAM), Jiangsu National Synergetic Innovation Center for Advanced Materials (SICAM), Nanjing Tech University (Nanjing Tech), 30 South Puzhu Road, Nanjing 211816, China. E-mail: wei-huang@njtech.edu.cn*

† Electronic supplementary information (ESI) available. See DOI: 10.1039/c6cp00273k

‡ These authors contributed equally to this work.

ability and application in high density memory devices. These attracted us to investigate the charge trapping properties and the mechanism of the sterically hindered organic semiconductor and search for more excellent materials for constructing non-volatile high density memory devices.

Here, we will focus on the charge trapping properties of a sterically hindered organic semiconductor SFDBAO, which exhibits potential application in memory devices.[19] To acquire high trapped charge density and long retention time, we try to blend SFDBAO and PS, which is widely used as an electret in memory devices for high charge storage ability.[25,26] Polymeric electrets have been used in high performance non-volatile organic field-effect transistor (OFET) memories due to their strong charge storage ability.[27] However, many electret materials show storage ability when the SiO_2 substrate is modified, which will need high voltage and hinder the development of flexible devices. In 2008, Wu *et al.* presented high-performance devices with donor-polymer blends as a buffer layer and provided a convenient approach for producing organic memory transistors at low cost and high efficiency.[28] Thus, in another work, we proposed that SFDBAO and electret PS were blended as the charge trapping layer to construct OFET devices. The performance of the device with the PS/SFDBAO trapping layer is better enhanced than that with SFDBAO. However, the effect of PS on the trapped electrons and holes is not clear; thus, it is very important to investigate the trapping and retention properties of electrons and holes in PS/SFDBAO films. In this work, we design the control experiments and visualize the process of trapped charges in films of PS and SFDBAO, and the blend of PS/SFDBAO by EFM to clarify the effect of PS on charge storage behaviors of PS/SFDBAO films. Through the qualitative and quantitative analysis, we compare the charge trapping properties of PS, SFDBAO and PS/SFDBAO blend films and find that the blend films possess high localization ability, good endurance and high trapped charge density. Otherwise, Au is deposited on the blend film and the potential profiles of the interface of Au and the blend are scanned by KPFM for charged and uncharged cases. The relaxation process of the trapped charges dependent on time and spatial distribution is discussed. The results exhibit that the utilization of an organic semiconductor and a polymeric charge storage electret blend as the trapped layer is a simple and promising strategy towards high performance non-volatile OFET memories.

2. Experiments

To achieve remarkable charge storage capability and excellent endurance, PS and SFDBAO with a molar ratio of SFDBAO/PS = 0.1 and 0.2 are mixed in a 5 mg ml^{-1} solution toluene and prepared on the cleaned 300 nm thick thermal SiO_2 grown on a highly doped n-type Si substrate using the spin-coating method at a spinning speed of 3000 rpm for 30 s. And then, the substrate was transferred to the oven to bake for 30 min at 80 °C in the air. The films of SFDBAO/PS = 0.1 and 0.2 are labeled as PS/SFDBAO-10%, and PS/SFDBAO-20% in the following work, respectively. The thickness of films is measured to be about 35 nm. To compare their charge trapping behaviors, SFDBAO and PS films of the same thickness are also prepared using the thermal vacuum evaporation method and the spin-coating method, respectively. The film morphologies of PS/SFDBAO-10%, PS/SFDBAO-20% and SFDBAO are recorded by using atomic force microscopy (AFM) in the tapping mode shown in Fig. 1(a)–(c). The films exhibit a homogeneous surface with root-mean-square roughness values of 0.223, 0.254, and 0.354 for PS/SFDBAO-10%, PS/SFDBAO-20%, and SFDBAO, respectively. By detecting their AFM topographic images at different times, we find that the stability of the SFDBAO film is worse than that of the blend films.

In this work, the experiments are performed using Bruker's Dimension Icon Atomic Force Microscopy under ambient conditions. Charges are injected by applying the controllable bias on the conductive AFM tip (Bruker's Pt/Ir coated probe tip with a resonant frequency 75 kHz and the spring constant 2.8 N m^{-1}) in the contact mode. During this period, the tip is brought into contact with the sample surface and maintained at a specific location for 10 s. The strong electric field between the tip and the sample induces an injection (for negative tip bias) or an extraction (for positive tip bias) of electrons from the tip to the sample by tunneling without obvious modification of the sample topography. Upon charging, the lateral distribution of trapped charges is monitored by scanning with EFM measurement, which can record the phase shift signal induced by the long-range electrostatic force gradient in the lift mode.[9,10] In the experiments, the lift height z between the tip and the sample is set to 50 nm for EFM scanning. The van der waals forces and the long-range electrostatic force interacting with the cone of the tip and the cantilever can be neglected.[10,16]

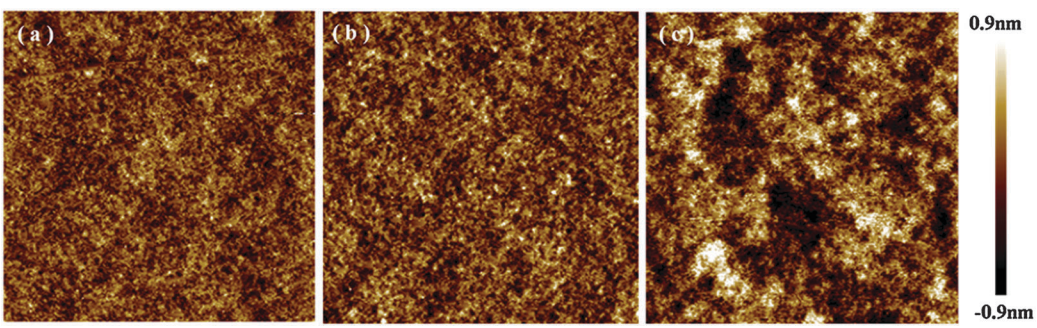

Fig. 1 AFM topographic images (3 μm × 3 μm) of (a) PS/SFDBAO-10%, (b) PS/SFDBAO-20% and (c) SFDBAO.

3. Results and discussions

Holes and electrons are injected on the films of SFDBAO, and PS/SFDBAO blends with different SFDBAO contents when the controllable injection biases are applied on tip. The topography and the local electrostatic force gradient are scanned by EFM simultaneously. In our work, little changes in the height of the signal or obvious variations in the EFM phase signal are detected after injection. Injection experiments on the blend films are carried out by varying tip biases from −10 V to +10 V in the contact mode. The typical EFM phase images of trapped charge spots injected with $V_{\text{i-tip}}$ = +8 V ($V_{\text{i-tip}}$ will be used to describe the injection tip biases) on SFDBAO, PS/SFDBAO-10%, PS/SFDBAO-20% films are presented in Fig. 2(a)–(c), respectively. The centerline cuts of corresponding charge spots are fitted with Gaussian curves and plotted in Fig. 2(d). The phase peak height (PH) and the full width at half-maximum (FWHM) of the Gaussian-type curve as shown in Fig. 2(d) will be used to describe the quantity of trapped charges and the width of the charge distribution, separately. From Fig. 2(d), one can see that PHs of the trapped charge spots with the same injection conditions are almost the same for SFDBAO, PS/SFDBAO-10%, and PS/SFDBAO-20% films. However, the corresponding FWHM order is as follows: PS/SFDBAO-20% film < PS/SFDBAO-10% < SFDBAO. It adequately illustrates that the charge carriers can be trapped in the localized region of these films, and the high localization property is shown in the blend of PS/SFDBAO-20%. It indicates that the blend of PS and SFDBAO can improve the localized ability of the trapped charges. We think that the interfaces between PS and SFDBAO in the PS matrix greatly restrict the lateral diffusion and enhance the localized ability of trapped charges.

For quantitative analysis, the sample and the tip, which can be treated as a circular disk generally, will constitute a parallel-plate-capacitor in the lift mode.[10,16,29–31] Therefore, based on the formula of force given in ref. 30 and 31, the relationship between the total trapped charges Q_s in films and the EFM signal phase shift $\Delta\varphi$ can be written as

$$\tan(\Delta\varphi) = -\frac{Q}{2k}\frac{\partial^2 C}{\partial z^2}{V_{\text{s-tip}}}^2 + \frac{Q_s Q}{2\pi k\varepsilon_0 z^2}\left(\frac{C}{z} - \frac{1}{2}\frac{\partial C}{\partial z}\right)V_{\text{s-tip}} - \frac{QQ_s^2}{2\pi k\varepsilon_0 z^3}$$

where Q is the quality factor of the probe and k is the spring constant of the cantilever. ε_0 is the permittivity of the vacuum. $V_{\text{s-tip}}$ is the scanning tip biases. C is the capacitor between the tip and the sample. From the above equation, the total amount of trapped charges Q_s can be calculated and the charge signs can also be confirmed using the method disscussed in the previous studies.[16,30,31] We scan the trapped charge spots by EFM with different scanning tip biases $V_{\text{s-tip}}$, and acquire the curve of $\tan(\Delta\varphi)$ dependent on $V_{\text{s-tip}}$, exhibiting that the holes/electrons are injected with positive/negative tip biases in these films. When $V_{\text{s-tip}} = 0$, the above equation can be simplified into a single electrostatic term, which is independent of the capacitance of the system. One can see that $\tan(\Delta\varphi)$ is approximately proportional to the square of the amount of trapped charges. Therefore, EFM measurements will be performed with $V_{\text{s-tip}} = 0$ to calculate the relative amounts of trapped charges. The corresponding trapped charge density can be acquired by dividing the amount of trapped charges by the effective area of the charge spots. Considering the homogeneity of the film and the stability of the ambient environment, the amount and density of trapped charges are the average values of ten different positions at the same sample in the following work.[22]

EFM phase signals of different injected charge spots for the films of PS/SFDBAO-10%, PS/SFDBAO-20%, and SFDBAO are scanned with $V_{\text{s-tip}} = 0$ and analyzed quantitatively. Related experiments for PS films have also been conducted. For example, the amount and density of trapped charges injected with +8 V and −8 V for these films are calculated and shown in Table 1. One can see that the amount of trapped positive/negative charges for all films is $\sim\times10^{-18}$ C. However, the trapped charge densities are dramatically different for the positively and negatively injected charge spots. For the negatively injected charges spots, the trapped charge density is about $\sim\times10^{-6}$ C m^{-2} for PS/SFDBAO-10%, PS/SFDBAO-20% and PS films. Here, we lack data of SFDBAO with the negative injection tip bias due to the fast diffusion rate of trapped charges. While as to the positive case, there is an obvious change of the trapped charge density from $\sim10^{-5}$ C m^{-2} to $\sim10^{-7}$ C m^{-2}, due to the difference of FWHM for trapped charge spots on different films. The trapped charge density of the PS/SFDBAO blend films ($\sim10^{-5}$ C m^{-2}) is an order of magnitude higher than

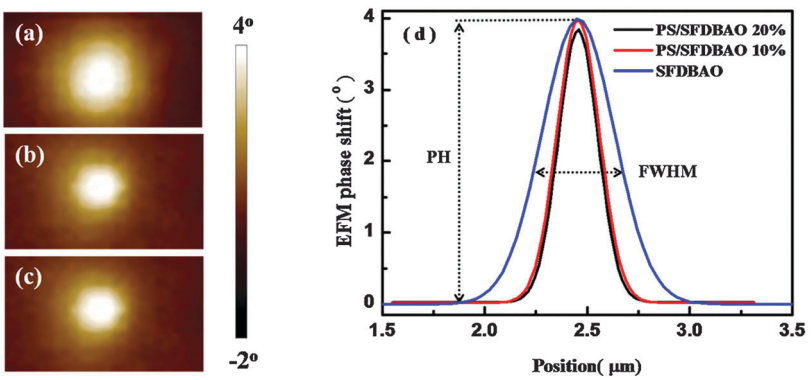

Fig. 2 EFM phase images (1 μm × 0.5 μm) of the trapped charge spots recorded on (a) SFDBAO, (b) PS/SFDBAO-10%, and (c) PS/SFDBAO-20% films after injection with $V_{\text{i-tip}}$ = +8 V. Centerline cuts of charge spots are fitted by Gaussian curve and shown in (d).

Table 1 Comparison of the quantity of trapped charges, trapped charge density and retention ability of PS/SFDBAO-10%, PS/SFDBAO-20%, SFDBAO, and PS for positive charges and negative charges

	The quantity of trapped charges (C)/trapped density (C m^{-2})		The PH decrease after injection 1200 s/3000 s	
Samples	Holes	Electrons	Holes	Electrons
PS	$(1.67 \pm 0.29) \times 10^{-18}/(1.58 \pm 0.16) \times 10^{-7}$	$(1.77 \pm 0.17) \times 10^{-18}/(1.96 \pm 0.39) \times 10^{-6}$	54%/∼	76%/∼
PS/SFDBAO-10%	$(2.02 \pm 0.33) \times 10^{-18}/(1.65 \pm 0.07) \times 10^{-5}$	$(2.04 \pm 0.14) \times 10^{-18}/(3.19 \pm 0.72) \times 10^{-6}$	28%/38%	82%/∼
PS/SFDBAO-20%	$(1.76 \pm 0.40) \times 10^{-18}/(1.95 \pm 0.63) \times 10^{-5}$	$(2.37 \pm 0.26) \times 10^{-18}/(1.83 \pm 0.18) \times 10^{-6}$	41%/62%	59%/83%
SFDBAO	$(2.51 \pm 0.18) \times 10^{-18}/(9.68 \pm 0.08) \times 10^{-6}$	∼/∼	63%/85%	∼/∼

the SFDBAO film ($\sim 10^{-6}$ C m^{-2}), and two orders of magnitude higher than the PS film ($\sim 10^{-7}$ C m^{-2}). It shows that the trapped density and localized ability of positive charges are greatly enhanced due to the blend of SFDBAO and PS.

To understand the diffusion of trapped charges, the charge spots have been scanned repeatedly at different times t after injection with controllable $V_{i\text{-}tip}$ on PS/SFDBAO-10%, PS/SFDBAO-20%, SFDBAO and PS films. We observe that the contrast of the trapped charge spots varies with time in EFM phase images, and we extract their PH and FWHM to describe the evolution of the trapped charges. The decays of PH and FWHM for charge spots injected with $V_{i\text{-}tip}$ = +8 V on the PS/SFDBAO-10%, PS/SFDBAO-20%, SFDBAO films, respectively, are exhibited in Fig. 3(a) and (b). The corresponding decay curves for $V_{i\text{-}tip}$ = −8 V are also exhibited in Fig. 4(a) and (b). For comparison, the relevant curves of the PS film are also inserted into Fig. 3(a), (b) and 4(a), (b).

One can see that the PH decreases greatly in the beginning and then remains relatively unchanged both in the case of $V_{i\text{-}tip}$ = +8 V and $V_{i\text{-}tip}$ = −8 V, exhibiting that the trapped holes and electrons in the films dissipate quickly at first, and then hold stability. However, the retention abilities of SFDBAO,

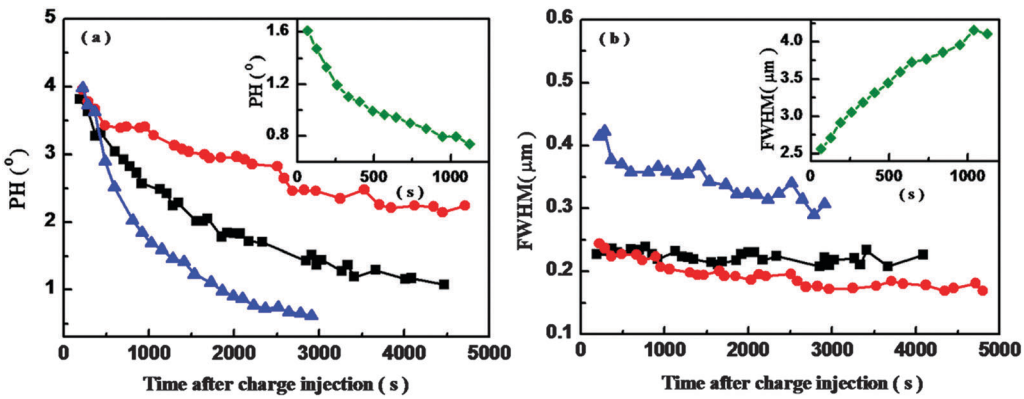

Fig. 3 Time evolutions of (a) peak height (PH) and (b) the full width at half-maximum (FWHM) extracted from EFM phase images for the charge spots injected with $V_{i\text{-}tip}$ = +8 V for 10 s on the PS/SFDBAO-10% blend film (circles), the PS/SFDBAO-20% film (squares), and on the SFDBAO film (triangles). The corresponding decay curves of the PS film are shown in the inset with diamonds.

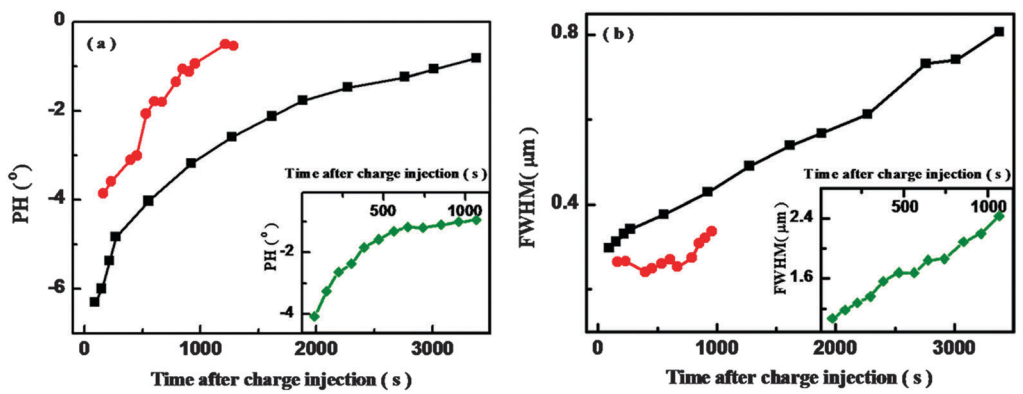

Fig. 4 Time evolutions of (a) peak height (PH) and (b) the full width at half-maximum (FWHM) extracted from EFM phase images for the charge spots injected with $V_{i\text{-}tip}$ = −8 V for 10 s on the PS/SFDBAO-10% blend film (circles), PS/SFDBAO-20% film (squares). The corresponding decay curves of the PS film are shown in the inset with diamonds.

PS/SFDBAO and PS films are different for holes and electrons. For the positive tip bias injection, Fig. 3(a) reveals that the peak height (PH) decreases by about 38%, 62%, 85% at 50 min after charge injection for PS/SFDBAO-10%, PS/SFDBAO-20%, and SFDBAO films, respectively. PS/SFDBAO-10% has the best endurance capacity in the films. Since we couldn't detect trapped charges in the PS film after 20 min of charging, we reveal the decrease (by 54%) of the peak height at 20 min after charging for the PS film also shown in Table 1, which is larger than that for PS/SFDBAO-10% (by 28%), and for PS/SFDBAO-20% (by 41%). It indicates that PS/SFDBAO blend films hold promising retention properties compared to SFDBAO and PS films, and the endurance of PS/SFDBAO-10% is better than that of PS/SFDBAO-20%. The retention time of PS/SFDBAO-10% is also longer than that of the SiO_2 film with silicon nanocrystals.[18,32] PS/SFDBAO-10% has also been used to construct memory devices with better device performances in our another work. For the negative tip bias injection, 82% and 59% decreases of PH for PS/SFDBAO-10% and PS/SFDBAO-20% are observed about 20 min after injection with $V_{i\text{-}tip} = -8$ V, respectively. While smaller decreases of 28% and 41% are calculated for PS/SFDBAO-10% and PS/SFDBAO-20% with positive charge injection $V_{i\text{-}tip} = +8$ V. What is mentioned above shows that the diffusion of electrons is quicker than that of the holes for SFDBAO and PS blend films. Otherwise, the degree of decrease of PH for PS is about 76% at 20 min after injection with $V_{i\text{-}tip} = -8$ V, which is larger than that for the PS/SFDBAO-20% film, but does not appear to be much different from that of the PS/SFDBAO-10% film. The results show that the blend of PS and SFDBAO has no obvious effect on increasing the endurance of trapped electrons, which is distinct from the case of trapped holes.

The evolution of FWHM is totally different between SFDBAO, PS, and PS/SFDBAO films. In Fig. 3(b), one can see that the initial FWHMs of trapped charge spots are 2.57 μm, 0.41 μm, 0.24 μm, and 0.23 μm for PS, SFDBAO, PS/SFDBAO-10%, PS/SFDBAO-20% films, respectively. FWHMs for the blend films are obviously smaller than those of PS and SFDBAO films. Besides, FWHMs of both PS/SFDBAO blends and SFDBAO films decrease at first and then tend to be stable, but the lateral spreading of charges is absent. However, the obvious lateral spreading is exhibited in the FWHM decay curve of PS as shown in the inset of Fig. 3(b). It is interesting to note that diffusion without lateral spreading in this study is entirely different from that reported in previous reports.[2,12,15,23,24] The results show that the blend of PS and SFDBAO leads to a strong positive charge confinement. It is a promising way to construct high density storage devices. For the negative injection conditions, the initial FWHMs of trapped charge spots for the blend films are 0.26 μm for PS/SFDBAO-10% and 0.30 μm for PS/SFDBAO-20% smaller than that for PS (1.07 μm), revealing that the blend films also lead to a high localization of negative charges. However, the blend films can't improve the lateral spreading of negative charges as shown in Fig. 4(b).

To further study the difference of diffusion properties between holes and electrons in the blend films, the OFET device is constructed without the organic semiconductor layer. The 50 nm thickness Au was thermally evaporated on the PS/SFDBAO-10% films through a shadow mask to form source and drain electrodes. The device sketch is shown in the inset of Fig. 5(a). Because this device does not have an active layer, usual transport measurements cannot be performed but the potential profile at the interface of the charge trapped layer and the Au electrode can be monitored by KPFM measurement under ambient conditions before and after charging at the Au electrode. KPFM has been used to characterize the electronic properties of materials and

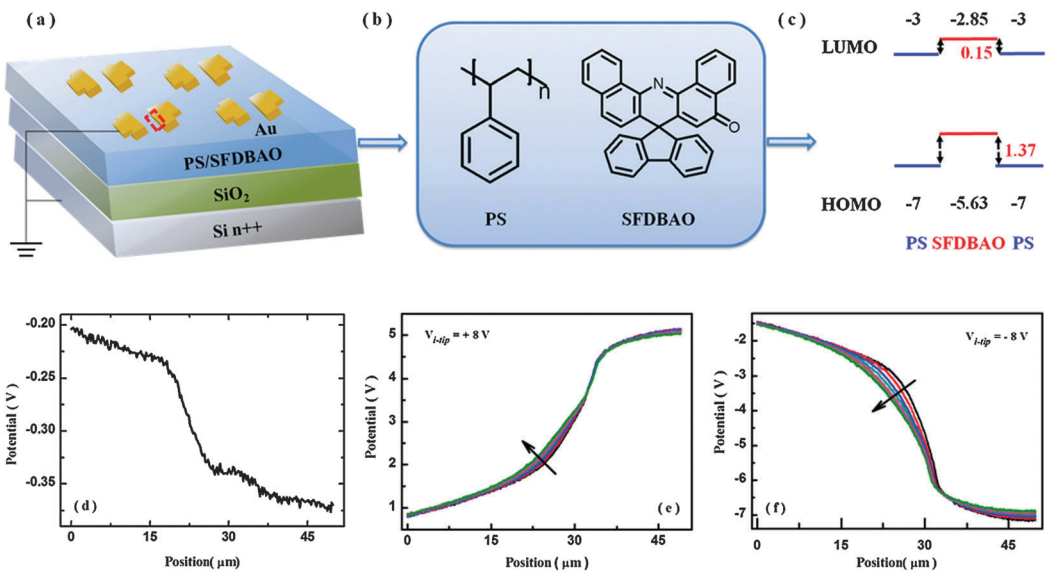

Fig. 5 (a) The schematic configuration of the used device in which an Au electrode and a gate electrode are grounded. (b) The molecular structures of PS and SFDBAO. (c) The energy level diagram of the PS/SFDBAO blend system. (d) The potential profile at the interface of Au and the PS/SFDBAO blend. In (e) and (f) the variations of potential profiles with time after the Au electrode in the dotted box injected with $V_{i\text{-}tip} = +8$ V and $V_{i\text{-}tip} = -8$ V are demonstrated. The time step between each curve is 43 s. The arrow directions represent the increase of time.

interface since it allows simultaneous high-resolution topographic imaging as well as electrical and electronic characterization.[9,10] It is commonly performed with two scan modes. The first scan collects the topographic signal in the tapping mode while the second scan, performed at a certain tip-surface distance, records the potential profile induced by the electrostatic force in the lift mode.

Before charging, the potential profile for the interface (marked by a red dotted line box in the inset of Fig. 5(a)) between the PS/SFDBAO film and the Au is scanned by KPFM with 80 nm lift height, shown in Fig. 5(d). One can see that the surface potential on the blend side is higher than on the Au electrode side about 0.15 V. And then, the relaxation process of the trapped charges is measured by KPFM after charges are injected with +8 V and −8 V tip biases on the right Au electrode in the red dotted box for 35 s, separately, while other electrodes are grounded as shown in Fig. 5(a). The time dependence of potential profiles is presented in Fig. 5(e) for the positive injection and Fig. 5(f) for the negative injection. The KPFM height signals show that there is no morphological change in the blend, Au, or at the interface due to charging, while the KPFM potential signals show that there are great changes in the potential profile. For the case of injection with +8 V on Au, surface potential on the blend side is lower than that on the Au side about 3.7 V, while after injection with −8 V, the surface potential on the blend side is higher than that on the Au side about 4.8 V. The potential difference between the charged and uncharged cases indicates that the charges are injected to the device, and the injection abilities for electron and holes are different. The changes of the surface potential as a function of time can also be observed in Fig. 5(e) and (f). One can see that the slopes of the potential profile at the interface increase with time. Here, the time step between two adjacent curves is 43 s. However, the variation of the slope at the interface in Fig. 5(f) is obviously greater than that in Fig. 5(e). This shows that the charges are embedded into the PS/SFDBAO blend film from Au over time, and the diffusion rate of electrons is quicker than that of holes in the PS/SFDBAO blend films.

The localization ability of trapped charges and the different diffusion properties between holes and electrons can be explained as follows. When SFDBAO is embedded in the PS matrix, it produces many interfaces not only in the horizontal direction but also in the vertical directions of the blend films. The interface is one of the major factors affecting the storage and release processes of trapped charges due to the potential barriers produced by the different HOMO (LUMO) energy levels at interfaces.[33] Thus, with the increase of the interfaces in the PS/SFBDAO blend film, the diffusion of trapped charges is greatly restricted, and the localized ability is enhanced as shown in Fig. 2(d).

From energy level diagrams in Fig. 5(c), the difference between the HOMO (LUMO) of PS and SFDBAO can be calculated as 1.37 eV (0.15 eV), which is the height of the potential barrier for holes labeled by Φ_{bh} (for electrons by Φ_{be}). One can see that Φ_{bh} can be the trap states for the holes, while Φ_{be} can't be for the electrons. We think that these extra trap states for the holes maybe one of the main reasons for the different storage, retention and diffusion processes of the trapped holes and electrons in the PS/SFDBAO blend films.

4. Conclusions

Charge trapping properties of the blend of PS and SFDBAO, pure SFDBAO and pure PS films are studied by EFM and KPFM measurements. The trapped charge density and the charge decay have been determined quantitatively from the visualized EFM phase signals. The results show that the blend films exhibit high localization ability, good endurance and high trapped charge density for not only holes but also electrons. However, the density, and diffusion rate for holes and electrons in the PS/SFDBAO blend films are totally different. By quantitative analysis, the trapped electrons density of PS/SFDBAO films is calculated to be 10^{-7} C m^{-2}, which has the same order of magnitude as PS and SFDBAO films, and the trapped hole density is 10^{-5} C m^{-2} for PS/SFDBAO, which is greater than that for PS and SFDBAO films. The lateral spreading of holes is limited due to the blend of PS and SFDBAO, while that of electrons is still observed in the blends as well as PS films. The diffusion rate of electrons is also different from that of holes. We suppose that the extra trap states for holes at the interface of PS and SFDBAO is the main reason for the differences of trapped holes and electrons. The determination of trapping properties and the decay process for both electrons and holes can be useful for the detailed characterization of PS/SFDBAO based high density memory devices.

Acknowledgements

This work was partially supported by the Science Foundation of Nanjing University of Post and Telecommunications (No. NY212031), National Natural Science Funds for Excellent Young Scholar (21322402), National Key Basic Research Program of China (973) (2015CB932200), National Natural Science Foundation of China (U1301243, 21274064), The Program for New Century Excellent Talents in University (NCET-11-0992), Doctoral Fund of Ministry of Education of China (20133223110007), Natural Science Foundation of Jiangsu Province (BM2012010), Synergetic Innovation Center for Organic Electronics and Information Displays, Excellent science and technology innovation team of Jiangsu Higher Education Institutions (2013) and Open Project from State Key Laboratory of Supramolecular Structure and Materials at Jilin University (sklssm2015022). This project was funded by the Priority Academic Program Development of Jiangsu Higher Education Institutions.

References

1 M. Cavallini, P. Stoliar, J. F. Moulin, M. Surin, P. Leclère, R. Lazzaroni, D. W. Breiby, J. W. Andreasen, M. M. Nielsen, P. Sonar, A. C. Grimsdale, K. Müllen and F. Biscarini, *Nano Lett.*, 2005, **5**, 2422.
2 S. Paydavosi, K. E. Aidala, P. R. Brown, P. Hashemi, G. J. Supran, T. P. Osedach, J. L. Hoyt and V. Bulović, *Nano Lett.*, 2012, **12**, 1260.
3 S. J. Kim and J. S. Lee, *Nano Lett.*, 2010, **10**, 2884.

4 M. Debucquoy, M. Rockelé, J. Genoe, G. H. Gelinck and P. Heremans, *Org. Electron.*, 2009, **10**, 1252.
5 Y. Yao, C. Li, Z. L. Huo, M. Liu, C. X. Zhu, C. Z. Gu, X. F. Duan, Y. G. Wang, L. Gu and R. C. Yu, *Nat. Commun.*, 2013, **4**, 2764.
6 Y. M. Kim, S. J. Kim and J. S. Lee, *IEEE Electron Device Lett.*, 2010, **31**, 503.
7 C. Sun, Z. Q. Lin, W. J. Xu, L. H. Xie, H. F. Ling, Y. M. Chen, J. Wang, Y. Wei, M. Y. Yi and W. Huang, *J. Phys. Chem. C*, 2015, **119**, 18014.
8 M. H. Jung, K. H. Song, K. C. Ko, J. Y. Lee and H. Lee, *J. Mater. Chem.*, 2010, **20**, 8016.
9 L. S. C. Pingree, O. G. Reid and D. S. Ginger, *Adv. Mater.*, 2009, **21**, 19.
10 V. Palermo, M. Palma and P. Samorì, *Adv. Mater.*, 2006, **18**, 145.
11 C. Y. Liu and A. J. Bard, *Chem. Mater.*, 1998, **10**, 840.
12 L. Ressier and V. L. Nader, *Nanotechnology*, 2008, **19**, 135301.
13 T. J. Dawidczyk, G. L. Johns, R. Ozgun, O. Alley, A. G. Andreou, N. Markovic and H. E. Katz, *Appl. Phys. Lett.*, 2012, **100**, 073305.
14 P. Annibale, C. Albonetti, P. Stoliar and F. Biscarini, *J. Phys. Chem. A*, 2007, **111**, 12854.
15 G. H. Buh, H. J. Chung and Y. Kuk, *Appl. Phys. Lett.*, 2001, **79**, 2010.
16 T. S. Jespersen and J. Nygård, *Nano Lett.*, 2005, **5**, 1838.
17 Z. L. Huo, L. Jin, Y. L. Han, X. K. Li, T. C. Ye and M. Liu, *Appl. Phys. A: Mater. Sci. Process.*, 2015, **118**, 1.
18 E. A. Boer, M. L. Brongersma and H. A. Atwater, *Appl. Phys. Lett.*, 2001, **79**, 791.
19 Z. Q. Lin, J. Liang, P. J. Sun, F. Liu, Y. Y. Tay, M. D. Yi, K. Peng, X. H. Xia, L. H. Xie, X. H. Zhou, J. F. Zhao and W. Huang, *Adv. Mater.*, 2013, **25**, 3664.
20 Y. C. Chiu, T. Y. Chen, C. C. Chueh, H. Y. Chang, K. Sugiyama, Y. J. Sheng, A. Hirao and W. C. Chen, *J. Mater. Chem. C*, 2014, **2**, 1436.
21 J. Y. Lin, W. Li, Z. Z. Yu, M. D. Yi, H. F. Ling, L. H. Xie, S. B. Li and W. Huang, *J. Mater. Chem. C*, 2014, **2**, 3738.
22 J. Wang, X. Wang, W. J. Xu, Z. Q. Lin, B. Hu, L. H. Xie, M. D. Yi and W. Huang, *J. Mater. Chem. C*, 2015, **3**, 12436.
23 N. Knorr, S. Rosselli and G. Nelles, *J. Appl. Phys.*, 2010, **107**, 054106.
24 C. Dumas, L. Ressier, J. Grisolia, A. Arbouet, V. Paillard, G. BenAssayag, S. Schamm and P. Normand, *Microelectron. Eng.*, 2008, **85**, 2358.
25 P. K. Watson, *IEEE Trans. Electr. Insul.*, 1995, **2**, 915.
26 J. C. Hsu, W. Y. Lee, H. C. Wu, K. Sugiyama, A. Hirao and W. C. Chen, *J. Mater. Chem.*, 2012, **22**, 5820.
27 Y. H. Chou, H. C. Chang, C. L. Liu and W. C. Chen, *Polym. Chem.*, 2015, **6**, 341.
28 W. Wu, H. Zhang, Y. Wang, S. Ye, Y. Guo, C. Di, G. Yu, D. Zhu and Y. Liu, *Adv. Funct. Mater.*, 2008, **18**, 2593.
29 C. Staii, A. T. Johnson, Jr. and N. J. Pinto, *Nano Lett.*, 2004, **4**, 859.
30 J. L. Zhang, X. L. Wu, Z. X. Gan, X. B. Zhu and Y. M. Jin, *Nano Res.*, 2014, **7**, 929.
31 J. J. McMorrow, C. D. Cress and C. A. Affouda, *ACS Nano*, 2012, **6**, 5040.
32 C. Y. Ng, T. P. Chen, H. W. Lau, Y. Liu, M. S. Tse and O. K. Tan, *Appl. Phys. Lett.*, 2004, **85**, 2941.
33 M. X. Dung, J. K. Choi and H. D. Jeong, *ACS Appl. Mater. Interfaces*, 2013, **5**, 2400.